Identification of a single plasma parcel during a radial alignment of the Parker Solar Probe and Solar Orbiter

Etienne Berriot, Pascal Démoulin, Olga Alexandrova, Arnaud Zaslavsky, Milan Maksimovic

A&A, 686, A114 (2024)
https://doi.org/10.1051/0004-6361/202449285

Astronomy & Astrophysics
Special issue

Solar Orbiter First Results (Nominal Mission Phase)

Identification of a single plasma parcel during a radial alignment of the Parker Solar Probe and Solar Orbiter

Etienne Berriot[1], Pascal Démoulin[1,2], Olga Alexandrova[1], Arnaud Zaslavsky[1], and Milan Maksimovic[1]

[1] LESIA, Observatoire de Paris, Université PSL, CNRS, Sorbonne Université, Université Paris Cité, 5 Place Jules Janssen, 92195 Meudon, France
e-mail: etienne.berriot@obspm.fr
[2] Laboratoire Cogitamus, rue Descartes, 75005 Paris, France

Received 19 January 2024 / Accepted 20 March 2024

ABSTRACT

Configurations in which two spacecraft, such as the Parker Solar Probe (PSP) and Solar Orbiter, are radially aligned provide opportunities for studying the evolution of a single solar wind parcel during so-called plasma line-ups. The most critical part of these studies arguably is the identification of what can be considered the same plasma crossing both spacecraft. We present here a method that allowed us to determine what we think to be the same plasma parcel that passed through PSP (~0.075 au) and Solar Orbiter (~0.9 au) after their radial alignment on April 29, 2021. We started by modeling the plasma propagation in order to obtain a first estimation of the plasma line-up intervals. The identification of the same density structure (with a crossing duration ~1.5 h) that passed through the two spacecraft allowed us to specify and confirm this estimate. Our main finding is that the density structure was very stable and remained well recognizable from PSP to Solar Orbiter despite its journey of ~137 hours in the inner heliosphere. We found, moreover, that the slow solar wind plasma parcel was significantly accelerated (from ~200 to ~300 km s^{-1}) during its propagation.

Key words. plasmas – Sun: heliosphere – solar wind

1. Introduction

The temperature of the solar corona is too high to remain in hydrostatic equilibrium. This leads to an expansion of the solar atmosphere in the interplanetary medium, which creates a supersonic and super-Alfvénic outflow of plasma that is called the solar wind (Parker 1958).

The solar wind is often separated into two categories depending on its speed. These are the fast and slow winds. The fast solar wind is thought to arise from coronal holes (Zirker 1977; McComas et al. 1998) and achieves speeds ranging from ~500 km s^{-1} to ~800 km s^{-1}. The slow solar wind has lower temperatures and higher densities than the fast wind, and has speeds ranging from ~150 km s^{-1} to ~500 km s^{-1}. The lowest solar wind speeds are only observed close to the Sun (Sanchez-Diaz et al. 2016; Maksimovic et al. 2020; Dakeyo et al. 2022). The processes that give rise to the solar wind and its exact origins are still disputed (see Abbo et al. 2016; Rouillard et al. 2021, and references therein). Many questions are also still pending regarding the radial evolution of the solar wind and the interplanetary structures it carries within the heliosphere.

The two spacecraft Helios 1 and 2 allowed the study of the radial evolution of what can be considered the same plasma as it passed through both spacecraft when they were radially aligned. This method was first employed by Schwenn et al. (1981a,b), who called it "plasma line-up". One of the intervals found by the authors was thoroughly studied by Schwartz & Marsch (1983) when Helios 1 and Helios 2 were situated at ~0.51 au and ~0.72 au from the Sun, respectively. Their study focused on the radial evolution of the energy budget and adiabatic invariants (Chew et al. 1956) in what was identified to be the same plasma parcel inside a fast solar wind stream. The authors also discussed different hypotheses and difficulties linked to the mapping and identification of the plasma parcel. The plasma parcel was identified considering a constant and radial propagation speed. However, any acceleration or nonradial flow can change the time intervals that are to be considered. Acceleration and nonradial flow are therefore potential sources of uncertainties.

Moreover, the terms "plasma line-up" and "plasma parcel" are somewhat ill-defined, as discussed in Schwartz & Marsch (1983). For example, the particle populations of the solar wind tend to propagate with different velocities. The protons often exhibit a beam in their velocity distribution function, the thermal speed of the electrons is much higher than their bulk speed, and alpha particles usually have a different bulk speed than protons (see Marsch 2012, and references therein). Furthermore, halo electrons are probably governed by nonlocal scattering mechanisms (Zaslavsky et al. 2024). We prefer to keep the general terminology "plasma parcel" and "line-up" throughout this study, however.

The recently launched missions Parker Solar Probe (PSP, Fox et al. 2016) and Solar Orbiter (Müller et al. 2020) are great new opportunities for line-up studies like this. Both spacecraft orbit simultaneously in the inner heliosphere, which allows combined observations and measurements (Velli et al. 2020). Conjoined observations with other spacecraft such as STEREO-A or BepiColombo are also possible (Hadid et al. 2021).

Some recent plasma line-up studies have been carried out, for PSP (0.1 au) and Solar Orbiter (1 au) by Telloni et al. (2021), and for PSP (0.17 au) and BepiColombo (0.6 au) by Alberti et al. (2022). The purpose of these studies was the radial evolution of the statistical properties of magnetic turbulence. Telloni et al. (2021) first estimated the intervals for the plasma line-up,

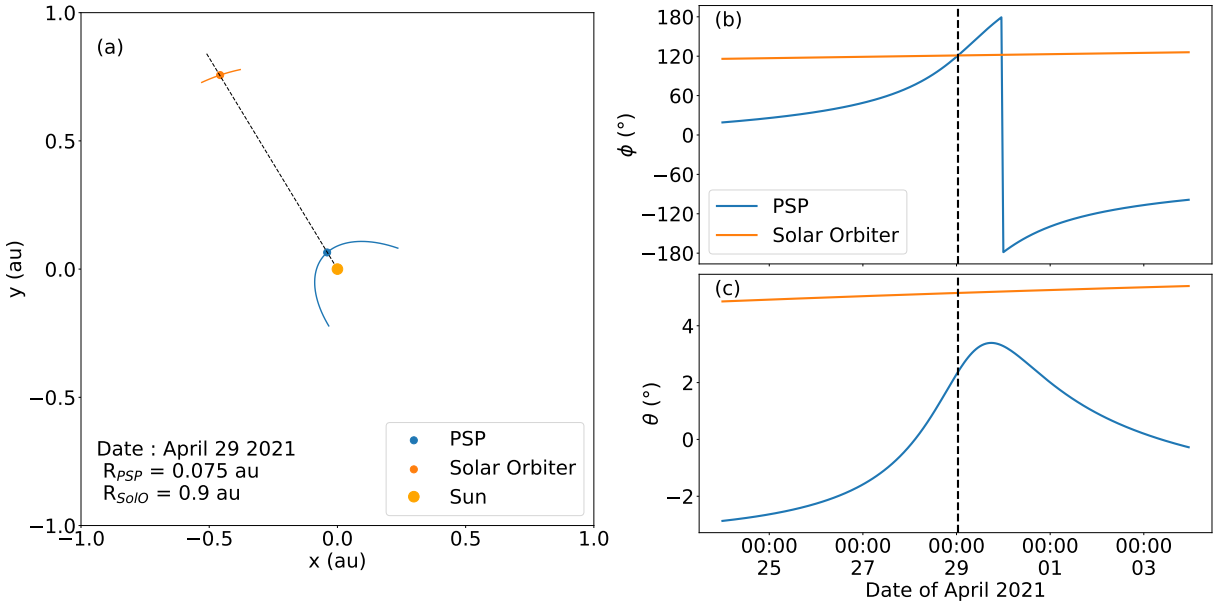

Fig. 1. Positions of the PSP and Solar Orbiter spacecraft around the studied line-up. Panel a shows the positions of PSP (blue) and Solar Orbiter (orange) on April 29, 2021 (dots) and the trajectories (lines) within the ecliptic plane between April 24, 2021 and May 4, 2021 as seen in an inertial reference frame centered on the Sun. The radial line from the Sun that passes through PSP and Solar Orbiter for the spacecraft coalignment time t_0 is indicated by the dashed black line. Panels b and c show the longitude ϕ, and latitude θ of PSP (blue) and Solar Orbiter (orange), respectively, as functions of time for the same interval as in panel a. We indicate the spacecraft coalignment time t_0 = 00 : 45 UT on April 29, 2021 as a vertical dashed black line in both panels.

assuming a constant speed of 315 km s^{-1} for the solar wind (as measured at PSP). They then assessed the plasma correspondence by calculating the Pearson correlation coefficient between measurements of the magnetic field magnitude by PSP and Solar Orbiter at time intervals corresponding to different propagation speeds ([250, 350] km s^{-1}) to take some possible acceleration into account. A similar method for the plasma propagation was employed in Alberti et al. (2022). The authors also based their identification on a cross-correlation method between the magnetic field magnitude measured by the two spacecraft, with sliding windows for both PSP and Bepi-Colombo and a calculation of the mutual information coefficient (Shannon 1948a,b; Cover & Thomas 2005). The identifications in Telloni et al. (2021) and Alberti et al. (2022) suggest a nearly zero acceleration of the solar wind during the propagation. This result was not verified because the solar wind velocity at the outer spacecraft in both studies was not measured. This is quite surprising as several statistical studies reported a non-negligible acceleration of the slow solar wind in the inner heliosphere (Schwenn et al. 1981a; Sanchez-Diaz et al. 2016; Maksimovic et al. 2020; Dakeyo et al. 2022).

The results of plasma line-up studies are highly dependent on the time intervals that are taken as being the same parcel of the solar wind. It is therefore crucial to be able to unambiguously identify what can be considered the same plasma at both spacecraft.

In this paper, we present a new approach that allowed us to identify the same plasma parcel as it passed through two radially aligned spacecraft. We studied the radial alignment between PSP (at ~0.075 au) and Solar Orbiter (at ~0.9 au) on April 29, 2021. The same plasma parcel was identified in several steps. We first present an overview of the spacecraft configuration in Sect. 2. Then, in Sect. 3, we describe our modeling of the solar wind propagation from the inner to the outer spacecraft to estimate the time intervals corresponding to the plasma line-up. Using this estimation, we identify the same density structure as it passed through PSP and Solar Orbiter in Sect. 4. We finally summarize our results and conclude in Sect. 5.

2. Data and line-up configuration

The goal of this study is to identify the same plasma parcel at two different distances from the Sun with PSP and Solar Orbiter. In order to do this, we took advantage of a configuration in which the two spacecraft are quasi-radially aligned, as shown in Fig. 1a, where we considered the positions of PSP and Solar Orbiter on April 29, 2021 around 01:00[1]. The plasma parcel was first crossed by PSP, then propagated outward, and was eventually crossed by Solar Orbiter after some propagation time τ.

For this configuration, PSP and Solar Orbiter were situated at approximately 0.075 au and 0.9 au from the Sun, respectively. We show in Figs. 1b and c the longitude (ϕ) and latitude (θ) of the two spacecraft around their radial alignment, defined as the time when they were both at the same longitude. We call this time t_0. It corresponds to

$$t_0 = \text{April 29, 2021 00 : 45 UTC}, \quad (1)$$

and this is used as the reference time for the remainder of this study. We therefore define

$$t = t_{\text{UTC}} - t_0, \quad (2)$$

where t_{UTC} is the coordinated universal time.

We show in Fig. 1b that the PSP longitude varies more than that of Solar Orbiter because PSP is orbiting much faster than

[1] The ephemerides were obtained from SPICE kernels (Acton 1996, https://naif.jpl.nasa.gov/naif/), for PSP (https://spdf.gsfc.nasa.gov/pub/data/psp/ephemeris/spice/) and Solar Orbiter (https://doi.org/10.5270/esa-kt1577e).

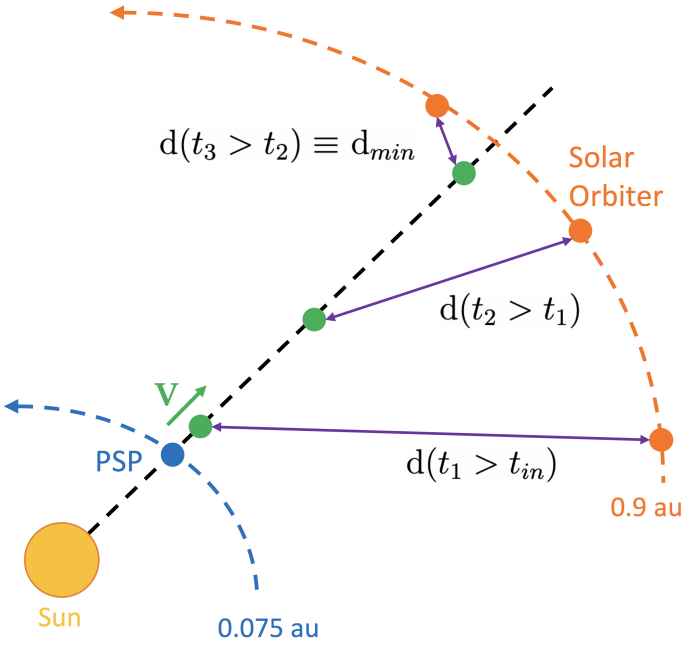

Fig. 2. Simplified schematic of the propagation method for a purely radial plasma speed (not to scale). The PSP position at a considered time t_{in} is indicated by the blue dot. We represent with green dots and at subsequent times (t_1, t_2, and t_3) the position of the plasma parcel that passed PSP at t_{in} and that propagated outward with $\boldsymbol{V}$ (green vector). We also represent the position of Solar Orbiter (orange dots) and the distance between the parcel and Solar Orbiter (double purple arrows) at the same times. The simplified trajectories of PSP and Solar Orbiter are shown by dashed blue and orange lines, respectively. The trajectory of the plasma parcel is shown by the dashed black line.

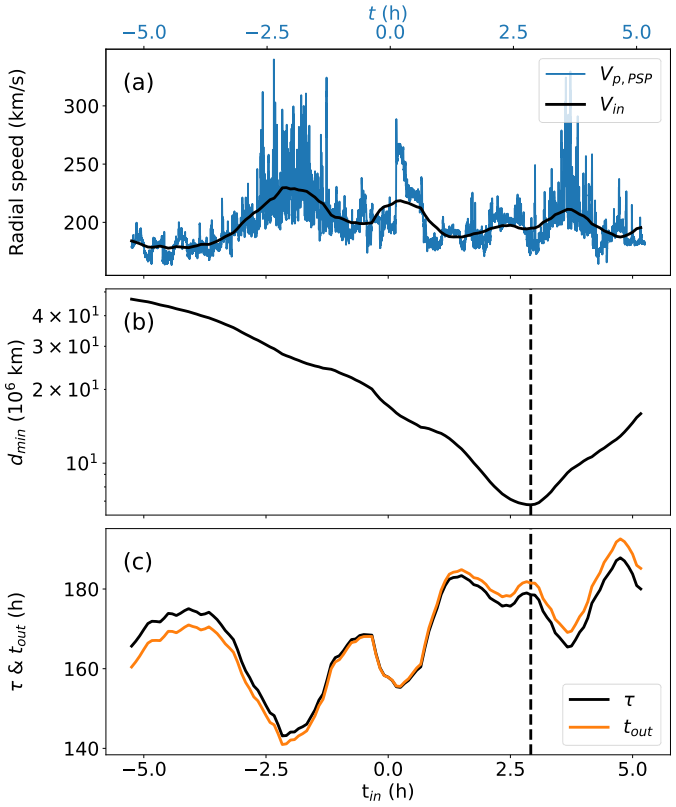

Fig. 3. Outcome of the propagation method for a radial and constant velocity $\boldsymbol{V} = (V_R = V_{\rm in}, 0, 0)$ in RTN coordinates. Panel a shows the radial proton speed recorded by PSP ($V_{\rm p,PSP}(t)$ in blue) and $V_{\rm in}(t_{\rm in})$ (in black), calculated as averages of $V_{\rm p,PSP}$ over $\Delta t = 1$ h centered on each considered $t_{\rm in}$. Panels b and c show the minimum distance $d_{\rm min}$ between the plasma parcel and Solar Orbiter and the corresponding propagation times τ (in black) and $t_{\rm out}$ (in orange), respectively. These are all functions of $t_{\rm in}$. The vertical lines in panels b and c correspond to the $t_{\rm in}$ for which $d_{\rm min}$ is minimum (called $d_{\rm MIN}$). All the time origins are set at t_0, corresponding to the radial alignment time of the spacecraft (Eq. (1)).

Solar Orbiter. This is due to PSP being about 12 times closer to the Sun than Solar Orbiter. At t_0, $\omega_{\rm PSP} \simeq 1.25 \times 10^{-5}$ rad s^{-1} and $\omega_{\rm SolO} \simeq 1.95 \times 10^{-7}$ rad s^{-1}, so that $\omega_{\rm PSP}/\omega_{\rm SolO} \sim 64$, where $\omega_{\rm PSP}$ and $\omega_{\rm SolO}$ are the angular speeds of PSP and Solar Orbiter, respectively.

We also point out the latitude difference of $\Delta\theta \sim 3°$ at t_0 when the two spacecraft are coaligned in longitude. At the distance of Solar Orbiter (~0.9 au), this difference corresponds to a length $l_{\Delta\theta} \simeq 7\,10^6$ km or 0.05 au. This $l_{\Delta\theta}$ imposes a lower bound on the scale of the plasma parcel we can expect to observe at both spacecraft.

For this study[2], we analyzed proton densities $N_{\rm p}$ and bulk velocities $\boldsymbol{V}_{\rm p}$ as well as the magnetic field B measured by PSP and Solar Orbiter. The proton parameters at PSP are obtained with measurements of the SPAN-ion instrument (Livi et al. 2021), which is part of the SWEAP (Kasper et al. 2016) suite. At Solar Orbiter, we use the total ion distributions from the Proton and Alpha particle Sensor (PAS, Owen et al. 2020). For the studied time intervals, the alpha to proton density ratio is of the order of 0.01 on both spacecraft. Thus, the PAS/SolO data used here represent mostly protons, even though they are computed from the total distribution functions. Magnetic field measurements are taken from the FIELDS instrument (Bale et al. 2016) on PSP and the MAG instrument on Solar Orbiter (Horbury et al. 2020).

[2] The data are publicly available at (https://spdf.gsfc.nasa.gov/pub/data/psp) for the PSP SWEAP and FIELDS (https://doi.org/10.48322/0yy0-ba92) measurements and at http://soar.esac.esa.int/soar/ for the Solar Orbiter SWA (https://doi.org/10.5270/esa-ahypgn6) and MAG (https://doi.org/10.5270/esa-ux7y320) measurements.

3. Ballistic propagation model

In order to identify the time intervals corresponding to a plasma line-up, the propagation of the plasma parcel from the inner to the outer spacecraft needs to be modeled first. There are several ways of doing this. We propose the following method.

We begin with the configuration shown in Fig. 1, for which the two spacecraft are quasi-aligned. The positions of PSP and Solar Orbiter as functions of time t are noted $\boldsymbol{R}_{\rm PSP}(t)$ and $\boldsymbol{R}_{\rm SolO}(t)$, respectively. We then define the position of the plasma parcel, $\boldsymbol{R}(t, t_{\rm in})$, at every moment t following its crossing of the inner spacecraft at a time $t_{\rm in}$,

$$\boldsymbol{R}(t, t_{\rm in}) = \boldsymbol{R}_{\rm in}(t_{\rm in}) + \int_{t_{\rm in}}^{t} \boldsymbol{V}(t', t_{\rm in}) {\rm d}t', \tag{3}$$

where $\boldsymbol{V}(t', t_{\rm in})$ is the plasma propagation velocity, which can have any profile, and by definition, $\boldsymbol{R}_{\rm in}(t_{\rm in}) = \boldsymbol{R}_{\rm PSP}(t = t_{\rm in})$.

We calculate the distance between the plasma parcel and the outer spacecraft as

$$d(t, t_{\rm in}) = |\boldsymbol{R}_{\rm SolO}(t) - \boldsymbol{R}(t, t_{\rm in})| \tag{4}$$

The process is schematized in Fig. 2. After some travel time $\tau(t_{\rm in})$, this distance passes by a minimum $d_{\rm min}(t_{\rm in})$ at a time $t = t_{\rm out}(t_{\rm in})$. We define the position of the plasma parcel after

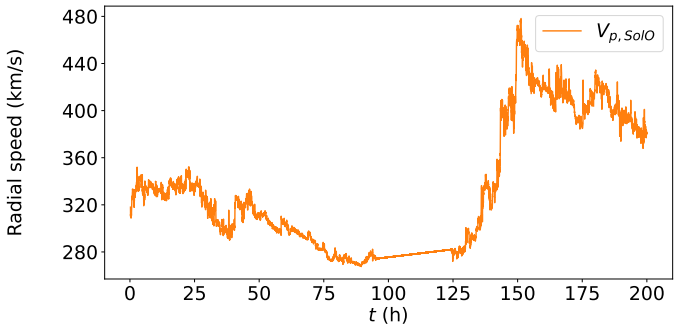

Fig. 4. Solar wind radial speed recorded by Solar Orbiter ($V_{\mathrm{p,SolO}}(t)$) for a time interval corresponding to $0 \leq t \leq 200$ h. The time origin is set at t_0 (Eq. (1)).

the travel as $\boldsymbol{R}_{\mathrm{out}}(t_{\mathrm{in}}) \equiv \boldsymbol{R}(t = t_{\mathrm{out}}, t_{\mathrm{in}})$. We next iterate the above computation for different t_{in}. Each considered time t_{in} is therefore linked to a time $t_{\mathrm{out}}(t_{\mathrm{in}})$ through the relation

$$t_{\mathrm{out}}(t_{\mathrm{in}}) = t_{\mathrm{in}} + \tau(t_{\mathrm{in}}). \tag{5}$$

This allows us to describe for every considered solar wind parcel, the time at which the plasma crossed by the inner spacecraft (at t_{in}) is closest to the outer spacecraft (at $t_{\mathrm{out}}(t_{\mathrm{in}})$), as well as the corresponding distance $d_{\mathrm{min}}(t_{\mathrm{in}})$ and propagation time $\tau(t_{\mathrm{in}})$.

3.1. Propagation method with constant velocity

We computed the propagation method described above with the following settings. We considered a set of starting times t_{in}, spaced by 5 min, each item of which defined the starting position of one plasma parcel. For every t_{in}, we defined the propagation velocity of the associated parcel as $\boldsymbol{V}_{\mathrm{in}} \equiv \langle \boldsymbol{V}_{\mathrm{p,PSP}} \rangle$, where $\langle \boldsymbol{V}_{\mathrm{p,PSP}} \rangle$ is the average proton velocity measured by PSP over a time interval Δt centered on t_{in}. We chose $\Delta t = 1$ h for a more relevant estimation of the plasma propagation speed by averaging velocity fluctuations related to the turbulent cascade. Finally, the plasma parcel positions were computed for every $t > t_{\mathrm{in}}$, with a one-minute resolution on t, and this was repeated for each t_{in}.

We show in Fig. 3 the results of this propagation method for the line-up configuration of Fig. 1. Figure 3a shows the radial proton bulk speed measured by PSP $V_{\mathrm{p,PSP}}(t)$ and the propagation speed $V_{\mathrm{in}}(t_{\mathrm{in}})$. Figure 3b gives the estimated distance between the plasma parcel and the outer spacecraft after the propagation, $d_{\mathrm{min}}(t_{\mathrm{in}})$, while Fig. 3c shows the corresponding propagation time $\tau(t_{\mathrm{in}})$ and time at the outer spacecraft $t_{\mathrm{out}}(t_{\mathrm{in}})$.

The closest approach is well defined: d_{min} has a clear minimum $d_{\mathrm{MIN}} = \min(d_{\mathrm{min}}) \simeq 7 \times 10^6$ km, indicated by the vertical dashed line. Therefore, the time intervals to search for at the inner and outer spacecraft should be around the associated $t_{\mathrm{in}} \simeq 2.9$ h and $t_{\mathrm{out}} \simeq 180$ h, respectively. We obtained $d_{\mathrm{MIN}} \simeq 7 \times 10^6$ km, which is close to $l_{\Delta\theta}$ (due to the spacecraft latitude difference around t_0) estimated at the end of Sect. 2. This is expected since the corresponding $t_{\mathrm{in}}(\simeq 2.9\,\mathrm{h})$ and $\tau(\simeq 180\,\mathrm{h})$ are much slower than the orbiting period of PSP and Solar Orbiter, respectively. Therefore, the spacecraft latitude difference $\Delta\theta$ does not change significantly from its value at $t = t_0$. Due to the large radial difference between the spacecraft, the speed variations observed at PSP (Fig. 3a), and therefore, on V_{in}, cause the propagation time $\tau(t_{\mathrm{in}})$ to vary strongly ($145\,\mathrm{h} \lesssim \tau \lesssim 185\,\mathrm{h}$) in the range of t_{in} we considered (see Fig. 3c).

We next examined the solar wind recorded by Solar Orbiter for a very wide range of times to determine how well the hypothesis of a constant speed is verified. We therefore show in Fig. 4 the radial proton speed recorded by Solar Orbiter for $0 \leq t \leq 200$ h. Unfortunately, no SWA data are available from ~05/02/2021 23:50 until ~05/04/2021 05:00, which translates into $90 \leq t \leq 125$ h. Regardless of the considered $t \in [0, 200]$ h, however, the observed proton speed at Solar Orbiter is higher than that at PSP. This is consistent with results of previous studies, which reported an acceleration of the slow wind in the inner heliosphere (Sanchez-Diaz et al. 2016; Maksimovic et al. 2020; Dakeyo et al. 2022). We therefore have to take this acceleration into account in the propagation method.

3.2. Propagation method with constant acceleration

Using the data at the two spacecraft alone, the in situ measured speeds can only define an average acceleration during the travel time. In the absence of other data, the simplest solution is to consider a constant acceleration constrained by the proton velocities measured by PSP and Solar Orbiter. However, this acceleration $\boldsymbol{a}$ is not directly accessible from the two sets of measurements because it first requires to link t_{in} and $t_{\mathrm{out}}(t_{\mathrm{in}})$ through the minimization of $d(t, t_{\mathrm{in}})$ (Eq. (4)) for each t_{in}. This is done below by scanning a range of $\boldsymbol{a}$ that is constrained by the observations. In order to simplify the notations, we mostly omit explicit mentions of the dependences on t_{in} in the remainder of this paper.

We first considered the plasma propagation with an arbitrary constant acceleration $\boldsymbol{a}$. For each t_{in}, the positions and speeds of the plasma parcel at every time $t > t_{\mathrm{in}}$ following the crossing of the inner spacecraft are given as

$$\begin{aligned} \boldsymbol{R}(t) &= \boldsymbol{R}_{\mathrm{in}} + (t - t_{\mathrm{in}})\boldsymbol{V}_{\mathrm{in}} + \frac{(t - t_{\mathrm{in}})^2}{2}\boldsymbol{a} \\ \boldsymbol{V}(t) &= \boldsymbol{V}_{\mathrm{in}} + (t - t_{\mathrm{in}})\,\boldsymbol{a}. \end{aligned} \tag{6}$$

After the propagation, this model provides

$$\boldsymbol{R}_{\mathrm{out}} = \boldsymbol{R}_{\mathrm{in}} + \tau\boldsymbol{V}_{\mathrm{in}} + \frac{\tau^2}{2}\boldsymbol{a} \tag{7}$$

$$\boldsymbol{V}_{\mathrm{out}} = \boldsymbol{V}_{\mathrm{in}} + \tau\,\boldsymbol{a}, \tag{8}$$

with τ the propagation time, $\boldsymbol{R}_{\mathrm{out}} = \boldsymbol{R}(t = t_{\mathrm{out}})$, and $\boldsymbol{V}_{\mathrm{out}} = \boldsymbol{V}(t = t_{\mathrm{out}})$. We use Eq. (8) to write the acceleration as

$$\boldsymbol{a} = \frac{\boldsymbol{V}_{\mathrm{out}} - \boldsymbol{V}_{\mathrm{in}}}{\tau}. \tag{9}$$

Replacing this in Eq. (7), we obtain

$$\tau = \frac{2\,\|\boldsymbol{R}_{out} - \boldsymbol{R}_{\mathrm{in}}\|}{\|\boldsymbol{V}_{\mathrm{out}} + \boldsymbol{V}_{\mathrm{in}}\|}.$$

Combining the last two equations, we can finally express the acceleration as

$$\boldsymbol{a} = \frac{\|\boldsymbol{V}_{\mathrm{out}} + \boldsymbol{V}_{\mathrm{in}}\|}{2\,\|\boldsymbol{R}_{out} - \boldsymbol{R}_{\mathrm{in}}\|}\,(\boldsymbol{V}_{\mathrm{out}} - \boldsymbol{V}_{\mathrm{in}}.) \tag{10}$$

When the same plasma is indeed crossed by the two spacecraft, we expect $\boldsymbol{R}_{\mathrm{out}} \approx \boldsymbol{R}_{\mathrm{SolO}}(t = t_{\mathrm{out}})$ and $\boldsymbol{V}_{\mathrm{out}} \approx \boldsymbol{V}_{\mathrm{p,SolO}}(t = t_{\mathrm{out}})$ after the propagation. $\boldsymbol{V}_{\mathrm{in}}$ can be estimated using $\boldsymbol{V}_{\mathrm{p,PSP}}(t)$ around t_{in} and $\boldsymbol{R}_{\mathrm{in}} = \boldsymbol{R}_{\mathrm{PSP}}(t = t_{\mathrm{in}})$. The acceleration written in Eq. (10) therefore only is a function of the observed quantities, provided that t_{in} and t_{out} are defined. However, it does not incorporate the association between t_{in} and t_{out} established by minimizing $d(t, t_{\mathrm{in}})$ of Eq. (4).

The results are expected to be close to the spacecraft alignment, and therefore, R_{in} and R_{out} are weakly dependent on the

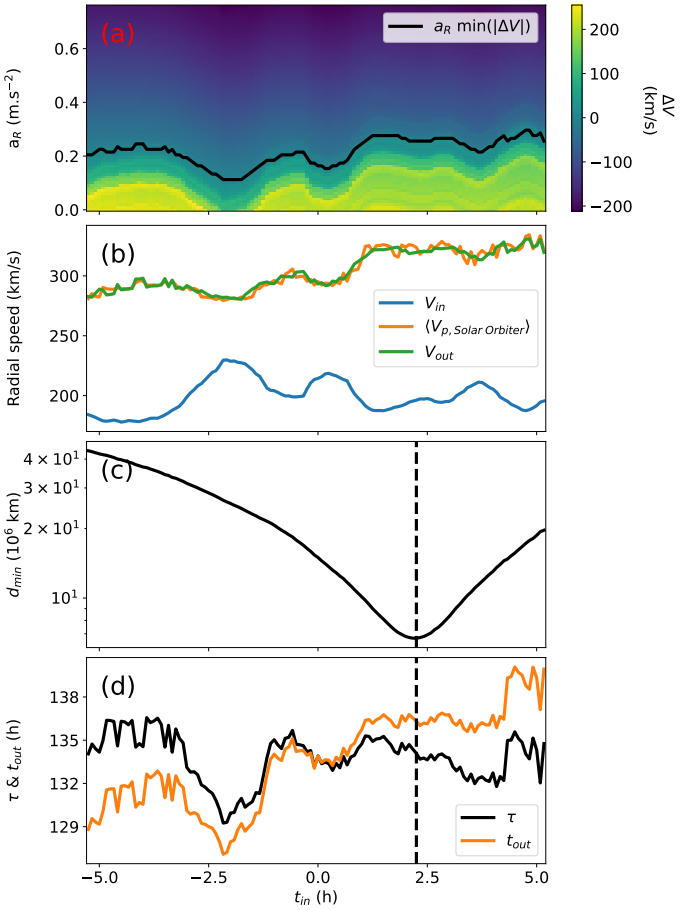

Fig. 5. Propagation method results using a constant acceleration a constrained by the observed plasma speeds at the inner and outer spacecraft. All quantities are shown as functions of $t_{\rm in}$. The colors in panel a are values of $\Delta V = \langle V_{\rm p,SolO}\rangle - V_{\rm out}$, and the black curve shows the radial acceleration for the minimum of $|\Delta V|$. The method results shown in panels b, c, and d all correspond to propagations considering this acceleration. Panel b shows in blue $V_{\rm in}$ calculated as in Fig. 3, in orange $\langle V_{\rm p,SolO}\rangle$ defined as the proton bulk speed measured by Solar Orbiter and averaged for $\Delta t = 1$ h centered on $t_{\rm out}$, and in green $V_{\rm out}$, which is the theoretical speed given by Eq. (8). The corresponding $d_{\rm min}$ is shown in panel c, and the corresponding τ and $t_{\rm out}$ are shown in panel d.

precise $t_{\rm in}$ and $t_{\rm out}$ values. We therefore calculated $\|\boldsymbol{R}_{\rm out} - \boldsymbol{R}_{\rm in}\|$ using the position of PSP around $t_{\rm in}$ and the position of Solar Orbiter around $t_{\rm out}$ (both associated with $d_{\rm MIN}$) estimated using a constant velocity (Fig. 3). This approximation is a posteriori justified by the fact that the $\|\boldsymbol{R}_{\rm out} - \boldsymbol{R}_{\rm in}\|$ estimated using a constant velocity and that estimated with a constant acceleration only differ by ∼1%. The acceleration given by Eq. (10) indeed mostly changes with $t_{\rm in}$ due to variations in $\boldsymbol{V}_{\rm in}$ and $\boldsymbol{V}_{\rm out}$.

As previously, we considered a purely radial plasma propagation and $V_{\rm in} = \langle V_{\rm p,PSP}\rangle$ averaged over $\Delta t = 1$ h around $t_{\rm in}$. The acceleration and speeds are noted as scalars representing the radial component of the vectors. Since the radial acceleration cannot be directly derived from observations, we defined a maximum acceleration a_{max} as

$$a_{\rm max} = \frac{V_{\rm out,max}^2 - V_{\rm in,min}^2}{2\,\|\boldsymbol{R}_{\rm out} - \boldsymbol{R}_{\rm in}\|}, \tag{11}$$

where we fixed $V_{\rm out,max} = 480\,{\rm km\,s^{-1}}$ and $V_{\rm in,min} = 180\,{\rm km\,s^{-1}}$ close to the maximum and minimum of the radial plasma speeds measured by Solar Orbiter and PSP, respectively, during the considered time periods. Then, for every $t_{\rm in}$, we computed 75 plasma propagations, all with a different constant acceleration. To do this, we considered acceleration values uniformly spaced between 0 and $a_{\rm max}$. By minimizing $d(t, t_{\rm in})$ for each a value, we obtained the parameters ($t_{\rm out}$, τ, $d_{\rm MIN}$) as functions of $t_{\rm in}$ and a.

We next defined the a value that is most compatible with the observed velocity at Solar Orbiter for each $t_{\rm in}$ value. The above model provides $V_{\rm out} = V(t = t_{\rm out})$ using Eq. (6) projected on the radial axis. Using Solar Orbiter measurements, we also defined (as for PSP) a proton bulk speed $\langle V_{p,SolO}\rangle$ averaged over $\Delta t = 1$ h around each obtained $t = t_{\rm out}$. We note that because of the data gap at Solar Orbiter (the straight line in Fig. 3d), we considered the missing data as interpolated values between the nearest available measurements. We therefore defined

$$\Delta V = \langle V_{\rm p,SolO}\rangle - V_{\rm out}. \tag{12}$$

Finally, for each $t_{\rm in}$, we selected the acceleration a that minimized $|\Delta V|$ so that the propagation model with a constant acceleration was most consistent with the observations at both spacecraft.

We show the results of the above procedure in Fig. 5. Panel a shows the values of ΔV, and the acceleration associated with the minimum of $|\Delta V|$ at each $t_{\rm in}$. Panel b shows the corresponding $V_{\rm in}$, $\langle V_{\rm p,SolO}\rangle$, and $V_{\rm out}$. The minimum of $|\Delta V|$ therefore is the difference between the green and orange lines. Its standard deviation is $\simeq 2\,{\rm km\,s^{-1}}$. This low value is an order of magnitude lower than the fluctuations of $V_{\rm in}$ and $\langle V_{\rm p,SolO}\rangle$. It shows that the acceleration bins are numerous enough.

The minimum distance $d_{\rm min}$ obtained for the minimum of $|\Delta V|$ is shown in Fig. 5c. As in Fig. 3, the vertical dashed line indicates the value $t_{\rm in}$ obtained for the minimum distance d_{MIN}. Here, $t_{\rm in} = 2.25$ h, which is smaller by only ∼40 min than the result obtained above with a constant velocity. When we consider a purely radial propagation speed and neglect 3D effects, the plasma line-up implies that the longitudes ϕ of the inner and outer spacecraft have to be the same at $t_{\rm in}$ and $t_{\rm out}$. When the longitude of the spacecraft line-up is used as the longitude origin, this condition approximately reads

$$\omega_{\rm out}\, t_{\rm out} = \omega_{\rm in}\, t_{\rm in}, \tag{13}$$

where $\omega_{\rm out}$ and $\omega_{\rm in}$ are the longitudinal angular velocities of the spacecraft around the Sun (in an inertial reference frame). This implies that a variation in $t_{\rm out}$, for instance, by $\delta t_{\rm out}$ due to a different transit time τ has an effect $\delta t_{\rm in} = (\omega_{\rm out}/\omega_{\rm in})\delta t_{\rm out}$ on $t_{\rm in}$. This means that a high angular velocity ratio $\omega_{\rm out}/\omega_{\rm in}$ between the two spacecraft due to a large difference in their distances from the Sun leads to low $\delta t_{\rm in}$. With the current PSP and Solar Orbiter configuration, the ratio $\omega_{\rm out}/\omega_{\rm in} \approx 1/64$. This explains why in the case we studied the $t_{\rm in}$ associated with the plasma line-up is weakly dependent on the plasma velocity profile.

Figure 5d shows τ and $t_{\rm out}$. These $t_{\rm out}$ values are fortunately not in the data gap shown in Fig. 4, so that the associated results are directly linked to Solar Orbiter observations. τ and $t_{\rm out}$ fluctuate much less than with a constant-speed hypothesis (Fig. 3c). More precisely, for a 10 h time interval of $t_{\rm in}$, the $t_{\rm out}$ variations are in a time interval of 15 h for a constant acceleration, compared to 50 h in the case of a constant velocity. Hence, the constant acceleration model (constrained by data from both spacecraft) provides a more reliable estimate of the time at Solar Orbiter for an approximate plasma line-up. The constant acceleration model also implies a significantly shorter propagation time τ. It is shorter by almost 50 h than the constant-velocity

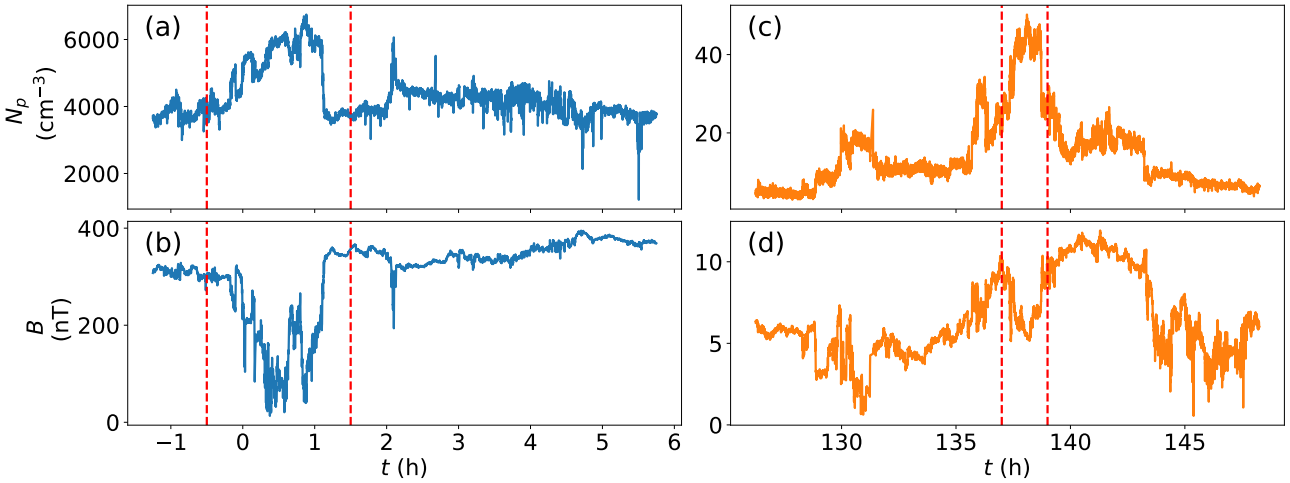

Fig. 6. Physical parameters measured by PSP and Solar Orbiter around the predicted plasma line-up. The proton density N_p is shown in panels a and c, and B, the magnitude of the magnetic field is shown in panels b and d. Blue curves (panels a and b) are PSP measurements around t_{in}, and oranges curves (panels c and d) are Solar Orbiter measurements around t_{out}, when the minimum distance d_{MIN} is achieved. Density structures are indicated between two vertical dashed lines, for $t \in [-0.5, 1.5]$ h and for $t \in [137, 139]$ h, in PSP and Solar Orbiter measurements, respectively.

model estimate (as expected because the observed plasma velocity increases).

Figure 5c shows that $d_{MIN} = 7 \times 10^6$ km (the minimum value of d_{min}) is well defined. This d_{MIN} is close to that obtained with a constant velocity (Fig. 3) and with the distance estimated in Sect. 2 due to the difference in spacecraft latitude around the spacecraft alignment ($l_{\Delta\theta} \sim 7 \times 10^6$ km). The fact that $d_{MIN} \simeq l_{\Delta\theta}$ confirms that when we consider a purely radial propagation velocity, this minimum is mainly constrained by the spacecraft orbits and not by the plasma dynamics. Moreover, the d_{min} curve with constant accelerations, Fig. 5c, is smoother than with constant velocities (Fig. 3b). This is a consequence of the narrower range of t_{out}, as shown in Fig. 5d.

4. Identification of the same plasma

4.1. Data selection

The propagation model provides a first estimate of the time intervals corresponding to the plasma line-up. This estimate has to be made more precise, however, and it must be confirmed. To do this, we propose to search for the same structure that passes through both spacecraft. When this is found, it can then be used as a marker to unambiguously define the same plasma.

Figure 6 shows the proton density N_p, and B the magnitude of the magnetic field measured by PSP (panels a, b) and Solar Orbiter (panels c, d) around the times corresponding to d_{MIN}, so $t_{in} = 2.25$ h and $t_{out} \sim 135$ h, as determined above (see Fig. 5d). We therefore chose to consider $t \in 2.25 \pm 4$ h for PSP and $t \in 135 \pm 10$ h for Solar Orbiter to take the uncertainties linked to the propagation model into account. The PSP measurements include a density enhancement and a simultaneous anticorrelated depletion in the magnetic field for $t \in [-0.5, 1.5]$ h. We note that a visual comparison with Solar Orbiter data already allows the identification of a very similar structure around $t \in [137, 139]$ h.

The proton density typically is indeed a useful parameter as it often exhibits well-identifiable spatial structures. Density enhancements were reported in the solar wind (especially in the slow wind) using either remote-sensing instruments (e.g., Sheeley et al. 1997; Rouillard et al. 2010a; Viall & Vourlidas 2015) or in situ measurements (e.g., Viall et al. 2008; Rouillard et al. 2010b; Stansby & Horbury 2018). These structures are thought to emerge near the tip of coronal helmet streamers. They are also generally thought to be well conserved during their propagation in the heliosphere and to be simply carried along with the surrounding solar wind (Kepko et al. 2016, 2024; Di Matteo et al. 2019), "like leaves in the wind" as put by Sheeley et al. (1997). However, we note that in contrast to leaves in the wind, these plasma structures in the solar wind are themselves part of the medium.

Moreover, mesoscale structures such as density enhancements have a typical radial size at 1 au of $\sim 5 \times 10^3 - 10^7$ km (Viall et al. 2021, and references therein). Then, the sizes of the larger density structures are comparable to the minimum distance d_{min} ($\in [1, 1.5] \times 10^7$ km for $t_{in} \in [-0.5, 1.5]$ h) evaluated for a propagation with constant acceleration. This implies that since Solar Orbiter is situated at ~0.9 au in the case we studied, one of these density structures could be large enough to eventually be crossed by both spacecraft. We note that d_{min} is most probably lower due to nonradial propagation effects (Appendix A). Furthermore, a direct comparison between the radial sizes of density structures (determined as $V_{p,R}\,\delta t$, with δt the duration of the structure) and d_{min} is only pertinent for structures with similar radial and ortho-radial extensions. Because the solar wind expands nearly spherically, the structures are expected to be elongated in the latitudinal and longitudinal directions at Solar Orbiter, however.

4.2. Association with the cross-correlations

The goal was to determine whether the structure identified at PSP (between two vertical dashed red lines in Figs. 6a,b) has also passed through Solar Orbiter. A common way to quantitatively assess the correspondence between the measurements at two spacecraft is to use a cross-correlation method. Using three different coefficients, we therefore computed the cross-correlation between PSP measurements for $t \in [-0.5, 1.5]$ h and intervals of same temporal lengths ($T = 2$ h) at Solar Orbiter for time shifts $125\,\text{h} \leq \tau \leq 145\,\text{h}$. We chose a time step of 0.1 h between each τ, defining the intervals at Solar Orbiter used for

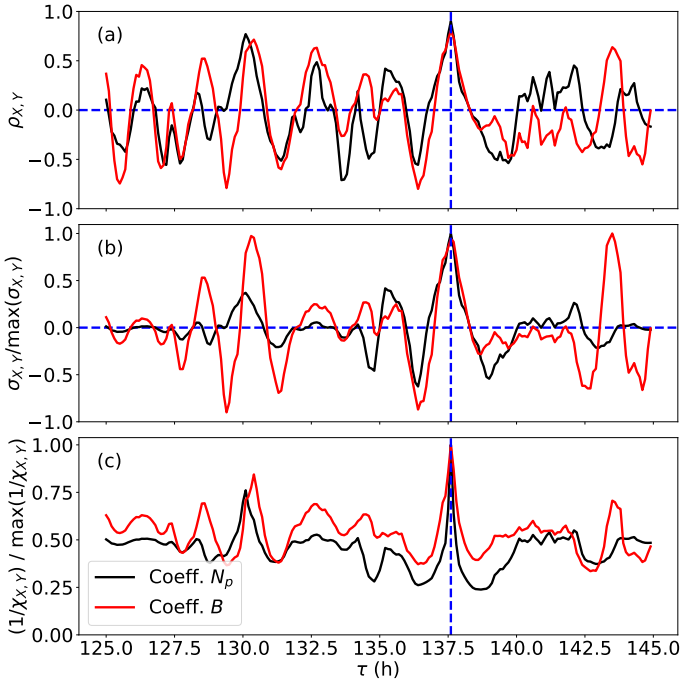

Fig. 7. Cross-correlation for measurements of the proton density N_p (black curves) and the magnetic field magnitude B (red curves) for PSP and Solar Orbiter using different measures. Panel a shows the Pearson correlation coefficient defined by Eq. (14), panel b shows the covariance, and panel c shows $1/\chi_{X,Y}$ defined by Eq. (17). The abscissa τ is the travel time between PSP and Solar Orbiter. The time interval considered at PSP is shown between dashed lines in Figs. 6a,c. The same time duration, 2 h, is used for the moving time window at Solar Orbiter.

the cross-correlation. We show the results in Fig. 7, where we computed these coefficients for the proton density N_p and for the magnetic field magnitude B.

Figure 7a shows the cross-correlation function based on the standard Pearson correlation coefficient $\rho_{X,Y}$, defined as

$$\rho_{X,Y}(\tau) = \frac{\langle \delta X(t)\, \delta Y(t+\tau)\rangle}{\sqrt{\langle \delta X(t)^2\rangle}\,\sqrt{\langle \delta Y(t+\tau)^2\rangle}}, \tag{14}$$

with

$$\begin{aligned} \delta X(t) &= X(t) - \langle X(t)\rangle \\ \delta Y(t+\tau) &= Y(t+\tau) - \langle Y(t+\tau)\rangle \end{aligned} \tag{15}$$

for $X(t)$ and $Y(t+\tau)$ the same physical parameter recorded by PSP and Solar Orbiter, respectively. The angle brackets denote averages over T (=2 h here). Due to its normalization, this coefficient is not affected by the amplitudes of X and Y, and it therefore tends to give a high correlation between structures of different amplitudes. This explains why we observe numerous high value peaks in Fig. 7a.

Figure 7b shows the cross-correlation function based on the covariance $\sigma_{X,Y}$, defined as

$$\sigma_{X,Y}(\tau) = \langle \delta X(t)\, \delta Y(t+\tau)\rangle, \tag{16}$$

which we normalized by its maximum over all the tested intervals ($\max(\sigma_{X,Y})$). In this way, the largest structures therefore tend to naturally give higher values for this coefficient because they have larger variances.

Table 1. Correlation coefficients between PSP and Solar Orbiter measurements for the proton density N_p and the magnetic field magnitude B at τ = 137.6 h (see the dashed line in Fig. 7 and Sect. 4.2).

	Correlation coefficients		
Physical Quantity	$\rho_{X,Y}$	$\frac{\sigma_{X,Y}}{\max(\sigma_{X,Y})}$	$\frac{1/\chi_{X,Y}}{\max(1/\chi_{X,Y})}$
N_p	0.90	1	1
B	0.81	0.97	1

Notes. Due to the normalization, a value of one for the coefficients using $\sigma_{X,Y}$ and $1/\chi_{X,Y}$ indicates an absolute maximum over the tested intervals.

Figure 7c shows the cross-correlation function based on the inverse of the chi-square coefficient $1/\chi_{X,Y}$, also normalized by its maximum over all the tested intervals, with $\chi_{X,Y}$ defined as

$$\chi_{X,Y}(\tau) = \sqrt{\langle (\delta X_c(t) - \delta Y_c(t+\tau))^2\rangle}. \tag{17}$$

$\chi_{X,Y}$ is named from its similarity with the statistical chi-square and should be minimum when the signals are most similar. We therefore chose to show $1/\chi_{X,Y}$ to more easily compare it with cross-correlation functions based on other coefficients. We used the typical radial variation summarized with a power law of the solar radial distance to define the normalized quantities $\delta X_c(t) = \delta X(t)\,(R_X/R_0)^{\varepsilon}$ and $\delta Y_c(t+\tau) = \delta Y(t+\tau)\,(R_Y/R_0)^{\varepsilon}$, where R_X and R_Y are the distance between the spacecraft and the Sun, and R_0 = 1 au is the distance taken for normalization. We fixed $\varepsilon = 2$ for the density and $\varepsilon = 1.6$ for the magnitude of the magnetic field in order to take the nearly spherical expansion of the plasma into account. Due to its spiral shape, the magnitude of the interplanetary magnetic field falls off less rapidly than R^{-2}. We therefore chose to correct B for a factor $(R/R_0)^{1.6}$, in accordance with previous statistical studies using Helios 1 data (Musmann et al. 1977; Schwenn & Marsch 1990). This correction is needed as the solar wind expansion strongly changes the magnitude of N_p and B with solar distance. Because of the subtraction $\delta X_c(t) - \delta Y_c(t+\tau)$, the results of Eq. (17) are sensitive to the choice of ε (or to any other normalization chosen for the signals). However, $1/\chi_{XY}$ is an important quantity because it shows far fewer peaks, and the main peak stands out more and is narrower than with the two other correlation coefficients. Finally, the three above coefficients are all linear, and any nonlinear evolution of the plasma is therefore not correctly taken into account.

All these cross-correlation functions show either absolute or local maxima for Np and B at τ = 137.6 h (Fig. 7). We show these values in Table 1. The fact that all three coefficients have high values like this for both N_p and B at τ = 137.6 h supports the correspondence between the two structures shown within the vertical dashed red lines in Figs. 6a–d.

Figure 7 shows that the correlation coefficients also exhibit local maxima for some other time shifts. The most remarkable maximum is at $\tau \sim 130$ h. Figures 6c,d show another density structure and associated magnetic field depletion around t = 130 h. The corresponding correlation values are lower, however, and a following visual inspection failed to find a clear correspondence between the structures. We therefore disregarded this density structure as being the same as that observed at PSP.

4.3. Justifications and limitations of the correlation method

In the previous subsection, several parameters involved in the correlation estimation were fixed. We justify this choice below

and present a more general way of computing the different correlation coefficients. We point out that in general, X and Y can be described as functions of several free parameters,

$$X = X(t^*, T_X, \delta t_X)$$
$$Y = Y(t^* + \tau, T_Y, \delta t_Y),$$

with t^* denoting the center of the time interval at the inner spacecraft, and τ the time shift between t^* and the center of the time interval at the outer spacecraft (propagation time). T_X and T_Y are the lengths of the time intervals, and we also introduce δt_X and δt_Y, the time resolution over which the X and Y data sets are to be resampled, respectively. The evaluation of the correlation coefficient requires that X and Y have the same number of values n, however. This adds the constrain:

$$\frac{T_X}{\delta t_X} = \frac{T_Y}{\delta t_Y} = n.$$

Therefore, any correlation coefficient $C_{X,Y}$ between two measurements X and Y should in general be computed as a function of all the free parameters,

$$C_{X,Y} = C_{X,Y}(t^*, \tau, T_X, T_Y, n).$$

In Sect. 4.2, we fixed and constrained these parameters using the hypotheses discussed below to obtain physically relevant results.

As previously specified, we set $t \in [-0.5, 1.5]$ h, fixing $t^* = 0.5$ h and $T_X = 2$ h. The goal was to select a prominent structure that passed through one of the spacecraft, to then search for and find it at the other spacecraft. We selected the structure on PSP first because for the plasma line-up, $t_{\rm in}$ is better defined than the associated $t_{\rm out}$, which depends more on the model selected to describe the plasma velocity (Sect. 3.2).

We also assumed that the selected structure had a global uniform evolution with a homogeneous acceleration during the propagation. As we show below (Fig. 9, Sect. 4.4), this implies that the duration of the structure is similar at the two spacecraft. The time window T (=2 h here) we used for the cross-correlation is therefore the same at both spacecraft, $T_X = T_Y = T$.

The temporal resolution is $T_X = T_Y$, so that $\delta t_X = \delta t_Y = \delta t$, and we chose $\delta t = 20$ s. We note that in our case, the cross-correlation results weakly depended on δt as long as $\delta t \ll T$. Finally, these constraints leave τ alone as a free parameter.

Written in this form, the set of Eqs. (14), (16), (17)) is valid for the special case of $T_X = T_Y$. These equations can simply be written in their generalized form, however, regardless of which signals X and Y composed of n samples X_i and Y_i, respectively, by replacing the angle bracket by $\frac{1}{n}\sum_i^n(\ldots)$ and $X(t)$ and $Y(t+\tau)$ by X_i and Y_i.

In summary, we have shown that the cross-correlation method can be misleading because high values for one (or several) coefficient do not necessarily imply that the same structure has been crossed by the two spacecraft. Therefore, this method has to be employed carefully, ideally on several (relevant) physical quantities and using different coefficients. Finally, although it can be helpful, the use of this method alone is not enough for a rigorous identification of the same plasma at two spacecraft. The identification can only be confirmed through a physical analysis of the measurements.

4.4. Local comparison of the structures

We show in Fig. 8 the proton density and the measurements of the magnetic field magnitude of PSP and Solar Orbiter for a propagation time $\tau = 137.6$ h, adjusted using cross-correlation methods, as described in Sect. 4.2. The measurements on PSP are plotted as functions of t over a 2 h time interval (between the two vertical dashed red lines in Fig. 6). Solar Orbiter measurements are plotted as functions of $t - \tau$ to obtain comparable signals, also over a 2 h time interval. We corrected $N_{\rm p}$ by a factor $(R/R_0)^2$ and B by a factor $(R/R_0)^{1.6}$, with R the spacecraft distance to the Sun and $R_0 = 1$ au (as in the definition of $\chi_{X,Y}$; see Section 4.2).

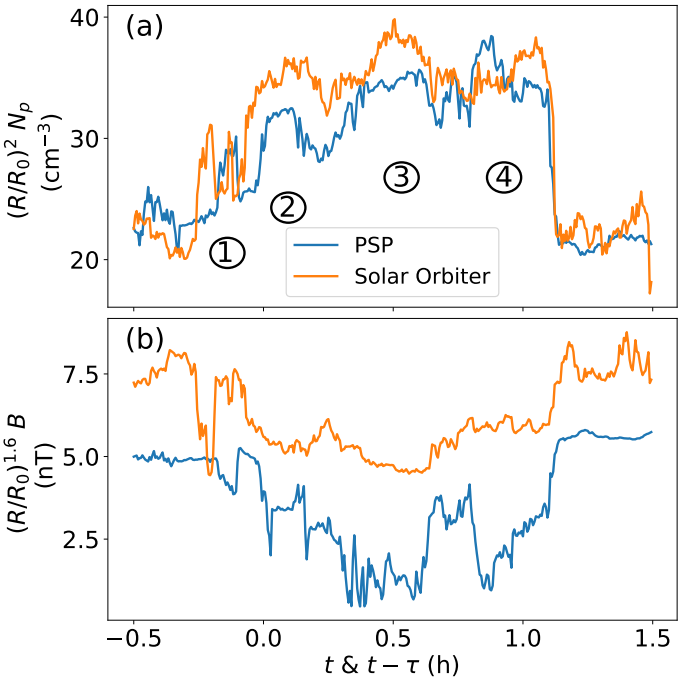

Fig. 8. Density structure measured by both PSP and Solar Orbiter. Proton density measurements (a) and magnetic field magnitude (b), corrected by a factor $(R/R_0)^2$ and $(R/R_0)^{1.6}$, respectively, to take the expansion from PSP (blue) to Solar Orbiter (orange) into account. The quantities are plotted as functions of t for PSP and as functions of $t - \tau$ for Solar Orbiter over a 2 h time interval (with $\tau = 137.6$ h as determined by several cross-correlation methods; see Sect. 4.2). An average over 20 s was applied to the data to better highlight the global behavior of the density structures.

We note that there is not only a global correspondence, as found in Fig. 7, but a correspondence on a finer scale is also present within the structures themselves (Fig. 8). This is especially noticeable for the plasma density. Of particular interest are four substructures that last between 0.1 and 0.3 h, which are detected at both spacecraft and numbered in Fig. 8a. This substructuring, with typical timescales of ~5–20 min, appear to be a common feature of solar wind density enhancements, and it is most probably linked with their generation process at the Sun (Di Matteo et al. 2019; Kepko et al. 2024). We also note that the density structure in both observations ends (at $t\&t - \tau \sim 1.1$ h) with a sharp decrease of a similar short duration and magnitude (when the spherical expansion is taken into account).

With radial velocities between 200 and 300 km s^{-1}, the duration of the four density substructures translates into spatial sizes L between 0.07 and 0.5×10^6 km, which is significantly smaller than the estimated minimum distance $d_{\rm MIN} \sim 7\times10^6$ km ($\sim 2\times10^6$ km when nonradial propagation is included (see Appendix A). Since L and $d_{\rm MIN}$ are size estimates in two orthogonal directions (R and N), we conclude that in order to be observed at both spacecraft,

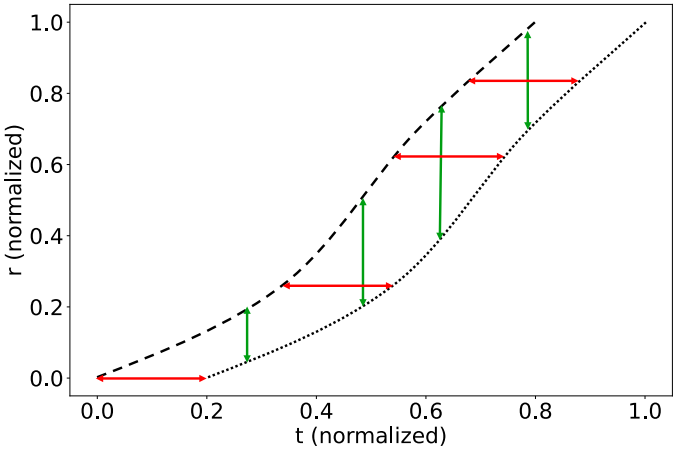

Fig. 9. Schematic illustration of a 1D structure propagation. The structure is delimited by its rear and front boundaries (with dashed and dotted lines, respectively). These boundaries are thought to have the same acceleration profile (so that the same forces act on them). We represent a general case with arbitrary acceleration and deceleration. Their normalized position (r) is shown as a function of the normalized time (t). The horizontal red arrows represent the time interval of the structure at a given radial position (as typical measurements provided by spacecraft). The vertical green arrows represent the spatial length of the structure at a given time.

the finer observed structures could be elongated by at least a factor of 4 in the N direction (about orthogonal to the ecliptic) as compared to the radial direction. However, the difficulty is to estimate the total amount of solar wind deflection in latitude precisely enough based only on velocity data measured at two locations of the trajectory (see Appendix A). Thus, the estimate of the extension ratio in the R and N directions of these finer density structures remains uncertain.

The physical parameters in Fig. 8 are shown as functions of time. This way of comparing measurements may appear arbitrary, but for a structure that varies along the radial direction, it appears the most relevant way, as described below. We show in Fig. 9 a schematic of the radial distance r as a function of time t between two points representing the front (dashed line) and rear (dotted line) boundaries of the structure. These two points have the same profile $r(t)$ up to a shift in time, as represented in Fig. 9. The spatial extent of the structure at a given time (green arrows) increases (or decreases) with time because the plasma accelerates (or decelerates). However, for each given position, the time extent of the structure (red arrows) remains constant, regardless of the acceleration profile. Therefore, when the acceleration profile is the same throughout the structure, and when the radial speeds of the spacecraft as compared to the solar wind speed are neglected, the time difference between two parts of the structure should remain the same at the inner and outer spacecraft. This behavior has previously been reported on a larger scale in Viall & Vourlidas (2015) using white-light images from COR2, the outer coronograph of STEREO. The authors observed a constant frequency (with a period of ~90 min) of periodic density structures released near the tip of helmet streamers, even though they were accelerated from ~90 to ~180 km s^{-1} within 2–15 solar radii. When the observed structure is considered to vary in the radial direction, the comparison in Fig. 8 of PSP and Solar Orbiter data within the same time interval (only shifted by the transit time) is justified.

The plasma structure we studied is shown in Fig. 8 and indeed lasts for a similar duration of ~1.5 h at the two spacecraft. When the mean relative radial plasma velocity (with respect to the spacecraft) is taken into account, this corresponds to a radial spatial scale of ~1.1×10^6 km and ~1.8×10^6 km at PSP and Solar Orbiter, respectively, which is about a factor 1.6 of the radial expansion between the two spacecraft. This radial expansion is much smaller than the expected longitudinal and latitudinal expansions (~$R_{\text{Solar Orbiter}}/R_{\text{PSP}} = 12$), however. Moreover, a radial stretching due to the solar wind acceleration would induce an additional decrease of N_p in general because for a spherical expansion, the continuity equation implies

$$\partial_R(N_\text{p} V_\text{p} R^2) = 0 \Rightarrow N_\text{p} V_\text{p} \propto R^{-2},$$

with ∂_R the partial derivative in the radial direction. This would need to be taken into account in general when the measurements are renormalized in order to compare them. We found in our case, however, that this decrease was coincidentally compensated for by a compression through the formation of a stream-interaction region (SIR). Observations of solar wind density structures that are swept up by SIRs have been reported in previous studies (Rouillard et al. 2010a,b; Plotnikov et al. 2016; Kepko & Viall 2019), and a more thorough analysis of this particular case will be presented in our next article.

5. Conclusions and perspectives

We presented our identification of what we think to be the same plasma (plasma line-up) that passes through PSP (~0.075 au) and Solar Orbiter (~0.9 au) after their radial alignment on April 29, 2021. We began by modeling the plasma propagation, considering a purely radial velocity, first with a constant speed using only PSP measurements (Sect. 3.1), and then with a constant acceleration (Sect. 3.2) constrained by the measurements of both spacecraft. This led to a first estimate of the time intervals corresponding to the plasma line-up. A visual inspection paired with the use of a cross-correlation method finally allowed us to identify (Sect. 4) the same density structure as it passed through both PSP and Solar Orbiter.

Our main finding here is how well conserved the identified density structure is despite its ~137 h journey from PSP (0.075 au) to Solar Orbiter (0.9 au). We were even able to associate substructures with temporal scales of about 10–20 min. There is also a (somewhat weaker) correspondence between the magnitude of the magnetic field at both spacecraft. This may simply be a consequence of a total pressure equilibrium in which the plasma pressure is mainly modulated by its plasma density.

In general, it might not always be possible to identify the same structure, even when the spacecraft pass through the "same plasma". In order to recognize the same plasma structure, several hypotheses have to be fulfilled, as we list below.

- The structure has to exist before it reaches the inner spacecraft.
- The structure should not be destroyed during its propagation, and it should also maintain its identity well enough to be unambiguously recognizable between the two spacecraft. For example, Borovsky (2021) presented some solar wind structures that were thought not to be destroyed under the effects of turbulence.
- The structure has to be large enough to pass through both spacecraft. Typically, mesoscale structures as described in Viall et al. (2021) (with radial sizes ranging from ~$5\,10^3$ km to ~10^7 km) have the right lengths for this, depending on the latitude difference between the two spacecraft.

Density enhancements generally fulfill these three conditions. They are thought to be created by reconnection in the solar

corona, and at least part of them is conserved during their propagation within the inner heliosphere. This is supported by element composition studies at 1 au (Kepko et al. 2016, 2024). Moreover, these structures can be large enough to pass through the two spacecraft, as described in Sect. 4.

Furthermore, the correspondence of the plasma structures at both spacecraft is best when the density measurements are compared as functions of time. This implies that the structure has mostly radial gradients and was accelerated with a somewhat homogeneous velocity profile throughout during the propagation (Fig. 9). Moreover, the discrepancies between the two recorded signals might not only be due to the structure evolution, but also to nonradial gradients. We recall that the two spacecraft orbit with different azimuthal velocities and were at different latitudes at the intervals we studied. In our case, the solar wind also developed nonradial velocity components during its propagation (Fig. A.1).

The association of plasma that passes through two spacecraft based on their in situ measurements alone can be difficult because the provided data represent 1D temporal cuts through temporally evolving 3D plasma. All the interpretations therefore strongly depend on the underlying assumptions made in order to compare these cuts. Here, 3D magnetohydrodynamics numerical simulations constrained with all possible data (in situ and remote sensing) would be of great help to further confirm the association and to help understand the physics involved. It could also give a more physically relevant estimate of the solar wind propagation than a ballistic model.

The constant acceleration obtained in Sect. 3.2 agrees with the average velocity profiles derived in Maksimovic et al. (2020) using Helios 1 and 2 measurements as close as 0.3 au. The more recent study of Dakeyo et al. (2022) using PSP and Helios 1 and 2 data showed, however, that the slow solar wind tends to have a steeper acceleration closer to the Sun on average (within $[0.1, 0.3]$ au). The modeling considering a constant acceleration might therefore not hold in a general case, and the fact that it is clearly relevant for our observations is probably due to the peculiarity of the identified intervals.

Last, the difference in latitude between the two spacecraft ($\sim 3°$) imposes a minimum distance $d_{\mathrm{MIN}} \simeq l_{\Delta\theta} \simeq 7 \times 10^6$ km (Sect. 3) that limits how close the plasma measured by the inner spacecraft can approach the outer spacecraft. A more realistic estimate considering the latitudinal plasma deflection (Appendix A) gives $d_{\mathrm{MIN}} \simeq 2 \times 10^6$ km. This deflection might have played a major role by bringing the plasma closer to the outer spacecraft. It is very likely that the structure would otherwise have missed Solar Orbiter and would have prevented the identification of the plasma line-up. The density enhancement, as well as its substructures, should indeed be more extended and coherent in the north-south direction than at this minimum distance d_{MIN}.

Finally, we only considered the proton density N_{p} and the magnitude of the magnetic field B. However, other physical parameters also show interesting behaviors that require a deeper analysis. This will be presented in a following study. We will show that the identified intervals correspond to crossings of the heliospheric current and plasma sheets (HCS and HPS). An SIR also developed during the plasma propagation, engulfed the HCS and HPS, and swept up the density structure.

Acknowledgements. We are grateful for the helpful comments from Nicholeen Viall as a referee of this article. The authors acknowledge funding support from CNES. We acknowledge the NASA Parker Solar Probe Mission, the SWEAP team led by J. Kasper. The FIELDS experiment on the Parker Solar Probe spacecraft was designed and developed under NASA contract NNN06AA01C. Solar Orbiter is a mission of international cooperation between ESA and NASA, operated by ESA. The Solar Orbiter Solar Wind Analyser (SWA) suite has been designed and created, and is operated by a large international consortium of institutes, which is led by UCL/Mullard Space Science Laboratory, UK, INAF-Istituto di Astrofisica e Planetologia Spaziali, Italy, Southwest Research Institute, USA and the Institut de Recherche en Astrophysique et Planétologie, France. These activities have been funded through numerous contracts from the UK Space Agency (UKSA), the UK Science and Technology Facilities Council (STFC), the Agenzia Spaziale Italiana (ASI), the Centre National d'Etudes Spatiales (CNES, France), the Centre National de la Recherche Scientifique (CNRS, France), the Czech contribution to the ESA PRODEX programme, and NASA.

References

Abbo, L., Ofman, L., Antiochos, S. K., Hansteen, V. H., et al. 2016, Space Sci. Rev., 201, 55
Acton, C. H. 1996, Planet. Space Sci., 44, 65
Alberti, T., Milillo, A., Heyner, D., Hadid, L. Z., et al. 2022, ApJ, 926, 174
Bale, S., Goetz, K., Harvey, P., et al. 2016, Space Sci. Rev., 204, 49
Borovsky, J. E. 2021, Front. Astron. Space Sci., 8, 131
Chew, G. F., Goldberger, M. L., & Low, F. E. 1956, Proc. Royal Soc. London Ser. A, 236, 112
Cover, T. M., & Thomas, J. A. 2005, Entropy, Relative Entropy, and Mutual Information (New York: John Wiley & Sons, Ltd), 13
Dakeyo, J.-B., Maksimovic, M., Démoulin, P., Halekas, J., & Stevens, M. L. 2022, ApJ, 940, 130
Di Matteo, S., Viall, N. M., Kepko, L., et al. 2019, J. Geophys. Res. (Space Phys.), 124, 837
Fox, N. J., Velli, M. C., Bale, S. D., et al. 2016, Space Sci. Rev., 204, 7
Hadid, L. Z., Génot, V., Aizawa, S., et al. 2021, Front. Astron. Space Sci., 8, 154
Horbury, T. S., O'Brien, H., Carrasco Blazquez, I., et al. 2020, A&A, 642, A9
Kasper, J., Abiad, R., Austin, G., et al. 2016, Space Sci. Rev., 204, 131
Kepko, L., & Viall, N. M. 2019, J. Geophys. Res. (Space Phys.), 124, 7722
Kepko, L., Viall, N. M., Antiochos, S. K., et al. 2016, Geophys. Res. Lett., 43, 4089
Kepko, L., Viall, N. M., & DiMatteo, S. 2024, J. Geophys. Res. (Space Phys.), 129, e2023JA031403
Livi, R., Larson, D. E., Kasper, J. C., et al. 2021, ESS Open Archive, 105, essoar.10508651
Maksimovic, M., Bale, S. D., Berčič, L., et al. 2020, ApJS, 246, 62
Marsch, E. 2012, Space. Sci. Rev., 172, 23
McComas, D. J., Bame, S. J., Barraclough, B. L., et al. 1998, Geophys. Res. Lett., 25, 1
Müller, D., St. Cyr, O.C., Zouganelis, I., et al. 2020, A&A, 642, A1
Musmann, G., Neubauer, F. M., & Lammers, E. 1977, J. Geophys. Zeitschrift Geophys., 42, 591
Owen, C. J., Bruno, R., Livi, S., et al. 2020, A&A, 642, A16
Parker, E. N. 1958, ApJ, 128, 664
Plotnikov, I., Rouillard, A. P., Davies, J. A., et al. 2016, Sol. Phys., 291, 1853
Rouillard, A., Davies, J., Lavraud, B., et al. 2010a, J. Geophys. Res., 115, A04103
Rouillard, A., Lavraud, B., Davies, J., et al. 2010b, J. Geophys. Res., 115, A04104
Rouillard, A. P., Viall, N., Pierrard, V., et al. 2021, in Solar Physics and Solar Wind, eds. N. E. Raouafi, & A. Vourlidas, 1, 1
Sanchez-Diaz, E., Rouillard, A. P., Lavraud, B., et al. 2016, J. Geophys. Res.: Space Phys., 121, 2830
Schwartz, S. J., & Marsch, E. 1983, J. Geophys. Res.: Space Phys., 88, 9919
Schwenn, R., & Marsch, E. 1990, Physics of the Inner Heliosphere I. Large-Scale Phenomena (Berlin: Springer-Verlag)
Schwenn, R., Mohlhauser, K. H., Marsch, E., & Rosenbauer, H. 1981a, Solar Wind, 4, 126
Schwenn, R., Mohlhauser, K. H., & Rosenbauer, H. 1981b, Solar Wind, 4, 118
Shannon, C. E. 1948a, Bell Syst. Tech. J., 27, 379
Shannon, C. E. 1948b, Bell Syst. Tech. J., 27, 623
Sheeley, N. R., Wang, Y.-M., Hawley, S. H., et al. 1997, ApJ, 484, 472
Stansby, D., & Horbury, T. S. 2018, A&A, 613, A62
Telloni, D., Sorriso-Valvo, L., Woodham, L. D., et al. 2021, ApJ, 912, L21
Velli, M., Harra, L., Vourlidas, A., et al. 2020, A&A, 642, A4
Viall, N. M., & Vourlidas, A. 2015, ApJ, 807, 176
Viall, N. M., Kepko, L., & Spence, H. E. 2008, J. Geophys. Res.: Space Phys., 113, A07101
Viall, N. M., DeForest, C. E., & Kepko, L. 2021, Front. Astron. Space Sci., 8, 139
Zaslavsky, A., Kasper, J. C., Kontar, E. P., et al. 2024, ApJ, 966, 60
Zirker, J. B. 1977, Rev. Geophys., 15, 257

Appendix A: Consistency with a nonradial propagation

In Section 3, the plasma line-up was calculated considering the solar wind propagation to be purely radial. This is not necessarily always justified because some phenomena can cause the solar wind to travel with nonradial components. We show in Figure A.1(a,b) that the proton bulk velocity has nonzero nonradial components around the identified plasma structures (especially for Solar Orbiter). We will show in our next study that this is due to the formation of an SIR. We therefore investigate the effect of these nonradial components on the modeled propagation below (Section 3.2). The goal here is to show whether when these effects are considered, the results are still consistent with the structure association reported in Section 4.2.

As in Section 3.2, we assumed a constant acceleration during the plasma travel. We considered the RTN referential of the inner spacecraft (PSP) at $t_{\rm in}$. Since the equations used to model the propagation are written in vector form, we can extend the method by also scanning a relevant range of acceleration in the T and N directions. The maximum acceleration values can be derived from Equation (10) following the same analysis as for Equation (11). This would require scanning a 3D space of parameters (a_R, a_T, a_N) to determine the minimum of d_{min}. While numerically well achievable, we provide below an analytical approach to deriving approximate estimates.

As a first approximation, and in order to highlight the different effects of the nonradial components, we independently considered the T and N velocity components. We therefore compared four different cases,

$$\begin{aligned}
\boldsymbol{V}(t) &= (V_R(t), 0, 0)\\
\boldsymbol{V}(t) &= (V_R(t), V_T(t), 0)\\
\boldsymbol{V}(t) &= (V_R(t), 0, V_N(t))\\
\boldsymbol{V}(t) &= (V_R(t), V_T(t), V_N(t))
\end{aligned}$$

with

$$V_j(t) = V_{in,j} + (t - t_{\rm in})\, a_j$$

for $j = R, T, N$.

As a second approximation, the radial acceleration (a_R) and starting velocity ($V_{R,in}$) were kept the same as those obtained by minimizing $|\Delta V|$ in Section 3.2 (see Figure 5). We also considered $\frac{\|\boldsymbol{V}_{\rm out}+\boldsymbol{V}_{\rm in}\|}{2\|\Delta\boldsymbol{R}\|} \simeq \frac{V_{out,R}+V_{in,R}}{2\|\Delta\boldsymbol{R}\|}$ because the radial velocity is about one order of magnitude higher than the transverse velocity components. This is equivalent to assuming that the propagation time of the plasma from the inner spacecraft to the nearest position of the outer spacecraft is mostly due to the radial component. The nonradial velocity components are large in the studied case (presence of an SIR; see our next study) as compared to the usual solar wind. Still, as shown below, the inclusion of these nonradial components does not significantly affect $t_{\rm in}$, τ and $t_{\rm out}$, so that the plasma line-up is achieved with similar sets of data for both spacecraft.

Using Equation (10), the nonradial acceleration components are written as

$$a_j = \frac{V_{out,R} + V_{in,R}}{2\|\Delta\boldsymbol{R}\|}\left(V_{out,j} - V_{in,j}\right) \tag{A.1}$$

with $j = T, N$. Since the association between the measurements at PSP and Solar Orbiter has already been made, we considered the nonradial speeds to be $V_{(in,out),j} = \langle V_{p,(PSP,SolarOrbiter),j}\rangle$ averaged over the time interval corresponding to the density structures. $\langle V_{p,(PSP,SolarOrbiter),j}\rangle$ are shown with horizontal dashed lines in Figure A.1(a,b). The primary goal here is to evaluate whether a nonradial propagation challenges the correspondence between the two density structures. This also means that the nonradial speeds and acceleration are less dependent on $t_{\rm in}$ and $t_{\rm out}$, allowing an easier interpretation of their effects on the propagation.

We show d_{min} and the corresponding τ as functions of $t_{\rm in}$ for the different velocity vectors in Figure A.1(c,d). In particular,

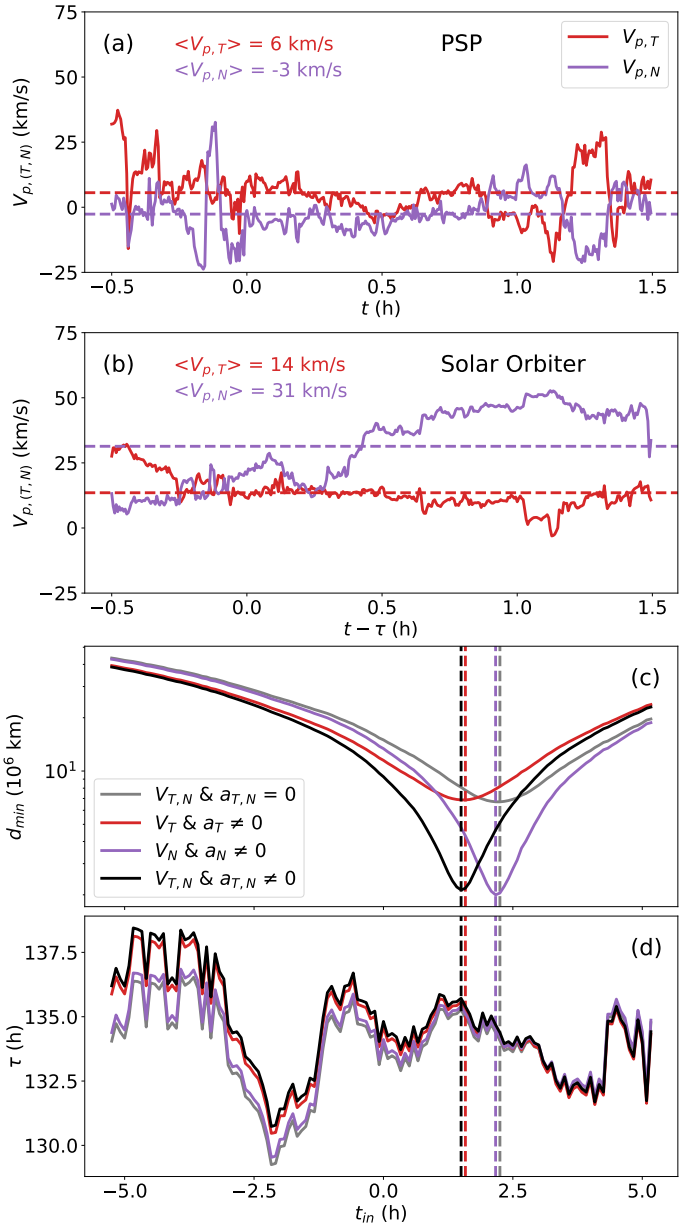

Fig. A.1. Effects of nonradial components on the predicted plasma line-up. Panels (a) and (b) show the $Vp_{,T}$ and $Vp_{,N}$ proton bulk speeds (red and purple curves, respectively) measured at PSP and Solar Orbiter for the same time intervals as in Figure 8. Panels (c) and (d) are the outcomes of the propagation method, as in Figure 5, including some nonradial components. The gray curves correspond to purely radial propagation, the red and purple curves correspond to propagation with nonzero T and N velocities and acceleration, respectively, and the black curves correspond to propagation with T and N components. For each propagation vector, the minimum distance $d_{\rm MIN}$ is marked by vertical dashed lines of matching color. The radial velocities and acceleration are the same as in Figure 5.

Figure A.1(c) shows that τ varies by ∼1 h at most when a nonradial propagation is considered. This justifies a posteriori that we kept a_R that we found in Section 3.2 and the use of Equation (A.1).

A modified V_T mostly affects the $t_{\rm in}$ associated with $d_{\rm MIN}$. Since the plasma has a finite propagation speed, a small difference in longitude is needed between the two spacecraft so that the outer spacecraft can intercept the closest possible plasma parcel. In this case, the plasma also propagates in the azimuthal direction, and therefore, $\boldsymbol{V}(t)$ now has a small longitudinal angle. Depending on the angel of this sign, the longitude difference needed between the two spacecraft decreases (positive angle) or increases (negative angle). This shifts the relation between d_{min} and $t_{\rm in}$ and almost does not change τ or d_{MIN} because the changes in the travel distance and latitude difference, respectively, are small. The shift is quite small due to the proximity of PSP to the Sun, which causes its longitude vary far more than that of Solar Orbiter (see Figure 1), and it rapidly covers the change in longitude difference that is due to the inclusion of a finite V_T.

A modified V_N changes d_{min} and therefore $d_{\rm MIN}$ (see Figure A.1(c)). As shown in Figure 1, PSP and Solar Orbiter have a small latitudinal difference $\Delta\theta$. As we discussed in Section 3, this difference implies a distance $d_{\rm MIN} \sim l_{\Delta\theta}$ when a purely radial propagation is considered. Adding a small positive V_N reduces this distance because the plasma covers part of the latitude difference during its propagation, which decreases $d_{\rm MIN}$ to $\sim 2\,10^6$ km. However, when the added V_N is too large (such that at $t_{\rm out}$, the plasma has a higher latitude than Solar Orbiter), then and increase in V_N would cause d_{min} and $d_{\rm MIN}$ to increase again (this is not the case for the current data).

In summary, each velocity and acceleration component mostly modifies one of the resulting parameters: τ (and $t_{\rm out}$) for V_R and a_R, $t_{\rm in}(d_{min} = d_{\rm MIN})$ for V_T and a_T, and $d_{\rm MIN}$ for V_N and a_N. The estimates for nonradial propagations are consistent with the identification of the structure (Section 4) and do not change the predicted time intervals for the plasma line-up by much. The inclusion of a positive V_N decreases $d_{\rm MIN}$, which reduces the estimated latitudinal extension of the structure. The inclusion of a positive V_T reduces the $t_{\rm in}$ associated with $d_{\rm MIN}$, bringing it closer to the observations, and it also reduces the required longitudinal extension of the structures. The inclusion of the T and N components implies a d_{min} curve (black in Figure A.1(c)) with a close $d_{\rm MIN}$ as when V_N and a_N are included (purple in Figure A.1 (c)), and at a nearby $t_{\rm in}$ as when V_T and a_T are included (red in Figure A.1 (c)). It is difficult to check the exact extent of the deflection because the profile of the real propagation speed is certainly more complex than we considered here. Moreover, V_T and V_N also vary throughout the structure and probably cause some distortion that would need to be taken into account.